

Realization of a tunable artificial atom at a supercritically charged vacancy in graphene

Jinhai Mao^{1†}, Yuhang Jiang^{1†}, Dean Moldovan², Guohong Li¹, Kenji Watanabe³, Takashi Taniguchi³, Massoud Ramezani Masir^{2,4}, Francois M. Peeters² and Eva Y. Andrei^{1*}

Graphene's remarkable electronic properties have fuelled the vision of a graphene-based platform for lighter, faster and smarter electronics and computing applications. One of the challenges is to devise ways to tailor graphene's electronic properties and to control its charge carriers^{1–5}. Here we show that a single-atom vacancy in graphene can stably host a local charge and that this charge can be gradually built up by applying voltage pulses with the tip of a scanning tunnelling microscope. The response of the conduction electrons in graphene to the local charge is monitored with scanning tunnelling and Landau level spectroscopy, and compared to numerical simulations. As the charge is increased, its interaction with the conduction electrons undergoes a transition into a supercritical regime^{6–11} where itinerant electrons are trapped in a sequence of quasi-bound states which resemble an artificial atom. The quasi-bound electron states are detected by a strong enhancement of the density of states within a disc centred on the vacancy site which is surrounded by halo of hole states. We further show that the quasi-bound states at the vacancy site are gate tunable and that the trapping mechanism can be turned on and off, providing a mechanism to control and guide electrons in graphene.

Supercriticality in atoms occurs when the Coulomb coupling, $\beta = Z\alpha$, exceeds a critical value of order unity, where Z is the atomic number and $\alpha \sim 1/137$ is the fine structure constant. In this regime the electronic orbitals, starting with the 1S state, sink into the Dirac continuum until Z is reduced to the critical value. This process, known as atomic collapse (AC), is accompanied by vacuum polarization and the spontaneous generation of positrons^{12,13}. But accessing this new physics requires ultra-heavy nuclei which do not exist in nature. In graphene, where the effective fine structure constant, $\alpha_g = \alpha(c/v_F) \sim 2$, is much larger, the critical coupling, $\beta_c = (Z_c/\kappa)\alpha_g = 0.5$, can be reached for a relatively modest charge^{6–10} (c is the speed of light, v_F the Fermi velocity and κ the effective dielectric constant). The transition to the supercritical regime in graphene is marked by the emergence of a sequence of quasi-bound states which can trap electrons. However, because graphene is a good conductor it is difficult to deposit and maintain a charge on its surface. Attempts to create charge by ionizing adatoms or donors with a scanning tunnelling microscope (STM) tip¹⁴ showed that the charge decays when the field is removed. Alternatively, ions can be deposited directly on graphene, but because the charge transfer is inefficient¹⁵, attaining the critical Z requires piling up many ions, which, in the absence of a controllable mechanism to overcome the Coulomb repulsion, is very challenging¹¹.

Here we show that a vacancy in graphene can stably host a positive charge. The charge is deposited by applying voltage pulses with an STM tip and its gradual build-up is monitored with scanning tunnelling spectroscopy (STS) and Landau level (LL) spectroscopy, and compared to numerical simulations. This ability to gradually charge the vacancy provides unprecedented control over the charge states, allowing one to explore *in situ* the evolution of the system from the subcritical to the supercritical regime. As the charge crosses into the supercritical regime we observe the sudden appearance of negative-energy quasi-bound electron states at the vacancy site, which mimic the bound states in an artificial atom. Seen as density of states (DOS) peaks below the Dirac point (DP) energy, E_D , these states produce a high intensity disc in the STS maps which is accompanied by a circular halo of hole states emerging at a larger radius. In addition to observing the lowest energy peak R1, which is the equivalent of the 1S atomic state reported previously¹¹, we observe two new states, R2 and R1'. R2 is the equivalent of the 2S atomic state and R1' is a new branch of collapse states arising from the broken sublattice symmetry at the vacancy site.

Vacancies were created by sputtering graphene with He⁺ ions^{16,17} and probed by STM and STS in a gated sample configuration shown in Fig. 1a (Methods). The STM topography in Fig. 1b shows that the initially smooth surface becomes peppered with bright defects. Zooming into a defect we observe the triangular $\sqrt{3} \times \sqrt{3}R30^\circ$ interference pattern (Fig. 1b, inset) characteristic of single carbon vacancies^{18,19}. This structure is absent in vacancies that are passivated by trapped ions, providing a clear topographic signature that distinguishes them from bare vacancies. Here, we focus only on unpassivated vacancies, as identified by their triangular structure in STM topography.

To evaluate the effect of a vacancy on the local DOS, we measured the spatial evolution of the differential conductance (dI/dV) shown in Fig. 1c²⁰. Far from the vacancy, the spectrum is 'V' shaped, with the minimum identifying the DP energy measured with respect to the Fermi energy, $E_F \equiv 0$. In contrast, on the vacancy site the spectrum features a sharp vacancy peak (VP) close to E_D , which is tightly localized within ~ 2 nm (Fig. 1c, inset)²¹. From the doping dependence of the VP (Fig. 1d), we find that its energy tracks the evolution of E_D with gate voltage, V_g , indicating that it is pinned to the DP and not to E_F (refs 19,22; Fig. 1e). This distinction is important for understanding the evolution of the spectra with charge and for identifying the supercritical regime.

According to recent density functional theory (DFT) calculations²³, the removal of a carbon atom from graphene and the subsequent lattice relaxation produces a positively charged

¹Rutgers University, Department of Physics and Astronomy, 136 Frelinghuysen Road, Piscataway, New Jersey 08855, USA. ²Departement Fysica, Universiteit Antwerpen, Groenenborgerlaan 171, B-2020 Antwerpen, Belgium. ³Advanced Materials Laboratory, National Institute for Materials Science, 1-1 Namiki, Tsukuba 305-0044, Japan. ⁴Department of Physics, University of Texas at Austin, Austin, Texas 78712, USA. [†]These authors contributed equally to this work. *e-mail: eandrei@physics.rutgers.edu

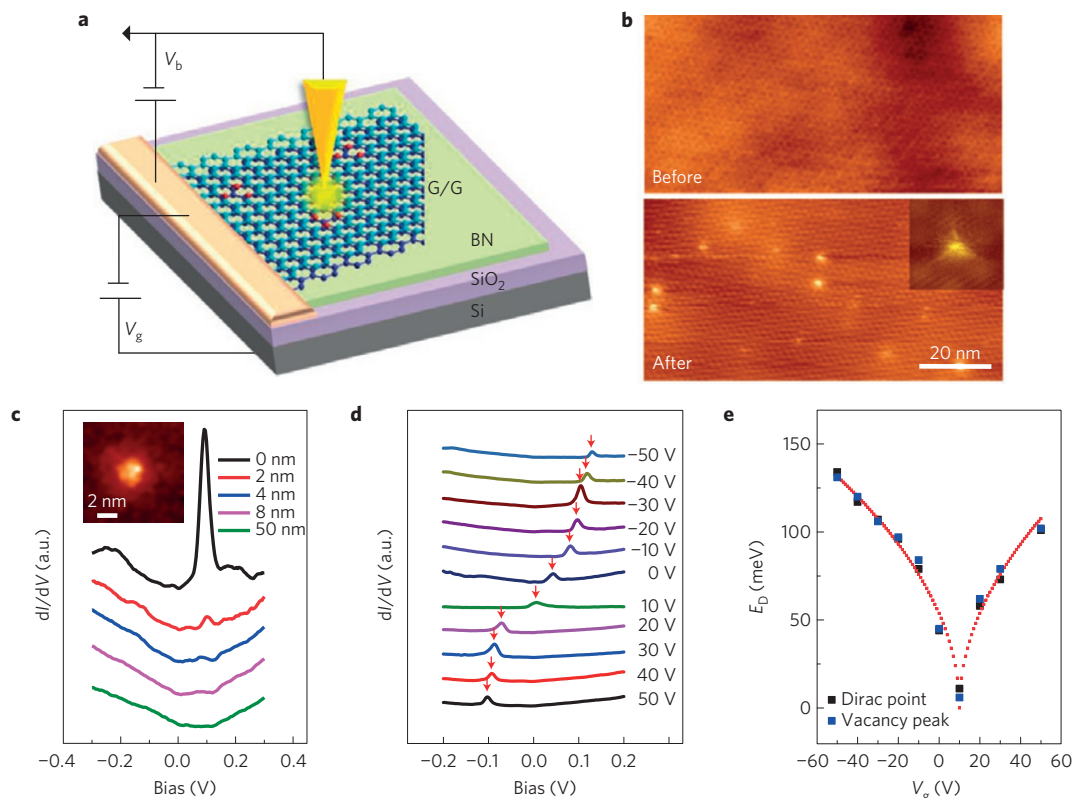


Figure 1 | Electronic properties of single vacancy on G/G/BN. **a**, Schematics of the experimental set-up. **b**, Typical STM topography of G/G/BN surface before and after He^+ ion sputtering. Inset: atomic resolution topography of a $4 \text{ nm} \times 4 \text{ nm}$ area containing a single vacancy shows the triangular interference pattern characteristic of a bare (unpassivated) vacancy. **c**, Spatial dependence of the dI/dV map at the energy of the VP. Experimental parameters for panels **b** and **c**: $V_b = -300 \text{ mV}$, $I = 20 \text{ pA}$, $V_g = -30 \text{ V}$. **d**, Doping dependence of the VP. The arrows label the Dirac point energy, E_D , of pristine graphene 50 nm away from any vacancy. Curves are offset for clarity. Tunnelling parameters: $V_b = -200 \text{ mV}$, $I = 20 \text{ pA}$. **e**, Gate voltage dependence of E_D (black) and VP energy (blue) relative to the Fermi energy ($E_F = 0$) extracted from the dI/dV spectra. The dotted line is a fit as detailed in Supplementary Section 2.

vacancy with effective charge $Z/\kappa \sim +1|e|$, where $|e|$ is the fundamental unit of charge. The effective charge and sign of a local vacancy in graphene can be directly estimated from LL spectroscopy, by measuring the on-site energy shift of the $N=0$ LL relative to its value far away, $\Delta E_{00} \approx -(Z/\kappa)(e^2/4(2\pi)^{1/2}\epsilon_0 l_B)$ (ref. 24). Here ϵ_0 is the permittivity of free space and l_B is the magnetic length. As we show in Supplementary Fig. 16s(b), this expression, obtained from first-order perturbation theory, is valid for $\beta > 0.1$, where it approaches the tight-binding result. In Fig. 2a we show a LL map along a line-cut traversing the vacancy. Contrary to expectations, we observed a negligible downshift, indicating that the vacancy charge is significantly smaller than that predicted by DFT. To estimate the local charge when it is too small to produce an observable LL downshift, we compare the splitting of the $N=0$ LL caused by the locally broken sublattice symmetry with numerical simulations (Supplementary Section 11 and Supplementary Fig. 16s(a)). The best fit to the data, shown in Fig. 2c, is obtained for a positively charged vacancy with $\beta \sim 0.1$. We next attempt to increase the vacancy charge by applying STM voltage pulses at its centre (Methods). It is well known that such pulses can functionalize atoms, tailor the local structure or change the charge state^{25,26}. In Fig. 2b we plot the LL map after applying several pulses. Now we observe a clear downshift in the $N=0$ LL, as expected for a positively charged vacancy with $\beta > 0.1$. Comparing with the theoretical simulation in Fig. 2d, we obtain a good match to the data for $\beta \sim 0.45$, which is also the value obtained from the formula above. The charge continues to build up as more pulses are delivered (Supplementary Fig. 6s). Interestingly, both

positive and negative pulses produce similar positively charged states (Supplementary Fig. 7s) and their charge is stable, remaining unchanged for as long as the experiment is kept cold. These results suggest that, similar to the numerical relaxation process applied in the DFT calculations²³, pulsing helps the system relax towards the ground state, which is the fully charged vacancy. The number of pulses needed to reach a given intermediate charge varies for different vacancies (Supplementary Fig. 6s), consistent with the stochastic process characterizing the relaxation. Importantly, applying a similar pulse sequence to pristine graphene produces no signature of charge build-up (Supplementary Fig. 8s). This indicates that the charge build-up occurs at the vacancy site itself and not in the substrate. Experiments were carried out on several samples and on different substrates, with pulsing producing similar results (Supplementary Section 6).

We performed numerical simulations, solving the tight-binding Hamiltonian for a charged vacancy (Supplementary Section 7), to calculate the evolution of the DOS with β . The simulations consider effects which go beyond the continuum limit and Dirac equation, such as the effect of a vacancy in graphene with broken electron-hole symmetry. This allows one to calculate the evolution of the local DOS well into the supercritical regime while including both the effects of the vacancy and magnetic field, which is not possible with continuum models. The results, summarized in Fig. 3a,b, show that at low β , in the absence of field, the spectrum consists of a single peak which evolves from the uncharged VP. With increasing β , the VP broadens and its energy becomes more negative, all the while remaining tightly localized on the vacancy site (Supplementary

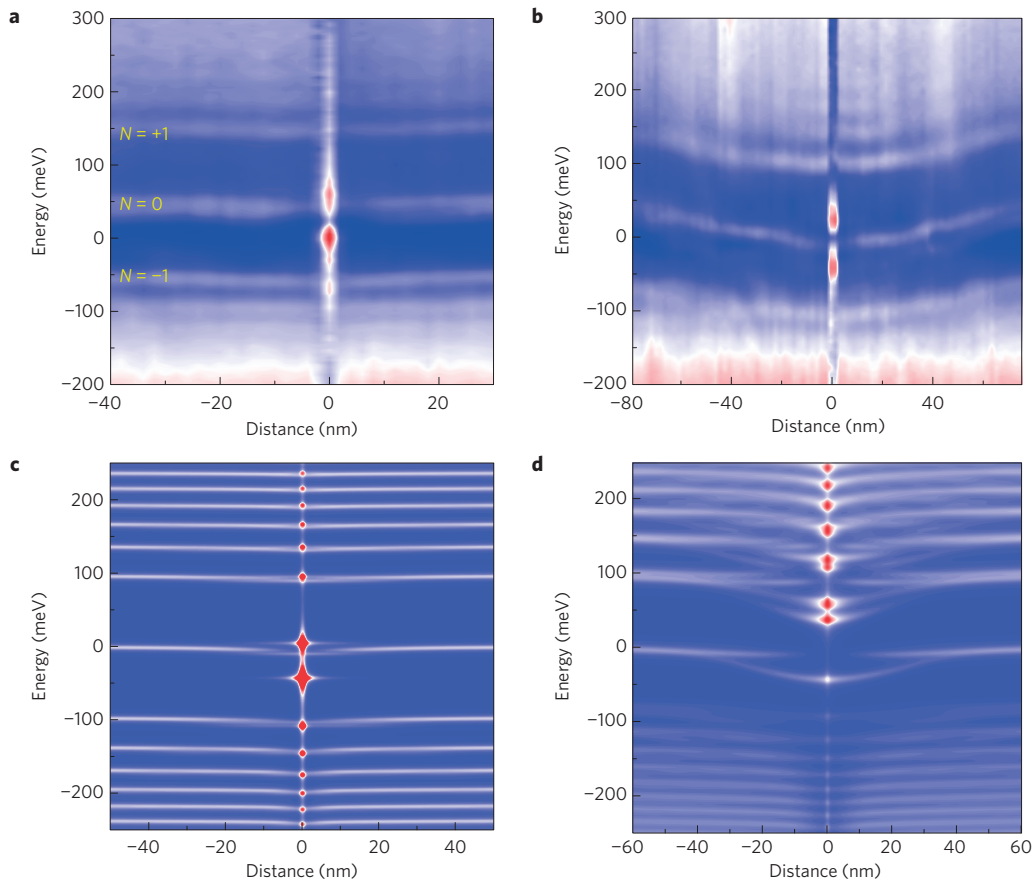


Figure 2 | Effect of charged vacancy on the Landau level (LL) spectra. **a,b**, Spatial dependence of the LLs across a line-cut traversing the vacancy before **(a)** and after **(b)** applying the voltage pulse. The position of the vacancy is marked by the enhanced intensity of the VP residing at its centre. The energy shift of the $N=0$ LL at 6 T, $\Delta E_{00} \sim 45$ mV, corresponds to an effective charge of $Z/\kappa \sim 0.2$ and $\beta \sim 0.45$, indicating that the charge is subcritical. We note that the $N=0$ LL is split at the vacancy site. Since the wavefunction for the $N=0$ LL is confined to one sublattice, the removal of one atom breaks the local symmetry and produces the strong splitting. **c,d**, Numerical simulation of spatial dependence of the LL spectra across a line-cut reproduces the experimental results in **a** and **b** for $\beta \sim 0.1$ and $\beta \sim 0.45$, respectively.

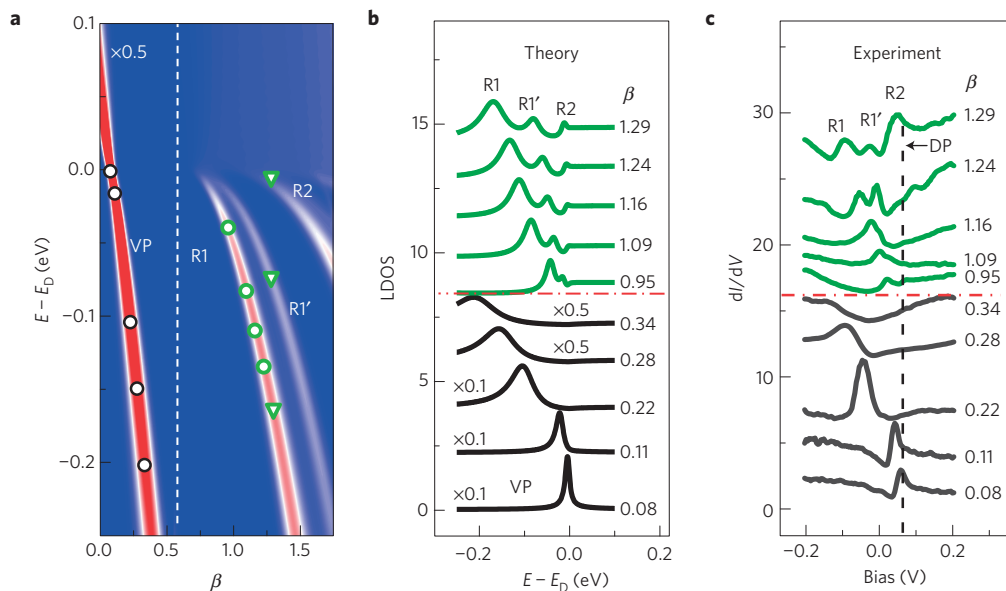


Figure 3 | Electronic properties of the charged vacancy. **a**, Simulated map of the evolution of the spectra with β . The intensity scale in the VP regime is divided by 2 to facilitate the comparison with the atomic-collapse (AC) regime. The symbols represent the energies of the VP and AC peaks from **c**. **b**, Simulated spectra for the β values in **c**. Curves are vertically offset for clarity. **c**, Evolution of STS with charge (increasing from bottom to top). Each curve is marked with its corresponding β value. The horizontal dashed line separates spectra in the subcritical and supercritical regimes. The vertical dashed line represents the bulk Dirac point (DP) measured far from any vacancy. Experimental parameters: $V_b = -200$ mV, $I = 20$ pA, $V_g = -54$ V.

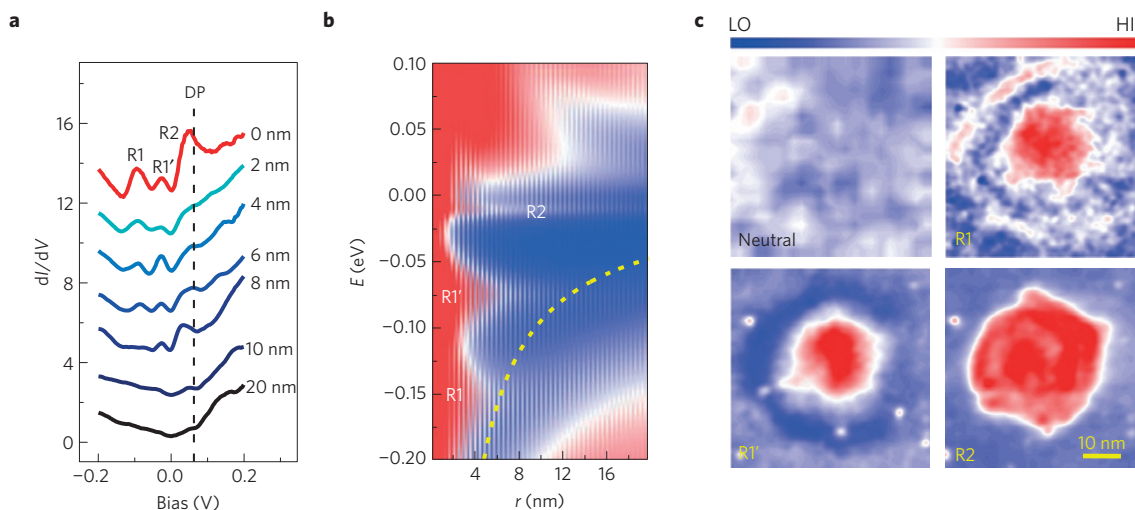


Figure 4 | Spatial evolution of the AC state. **a**, Spatial dependence of the AC states for $\beta = 1.29$. The dashed line labels the bulk DP. **b**, Spatial dependence of simulated spectra for $\beta = 1.29$. In the simulation, the bulk DP is taken as the energy origin. The dashed curve represents the local DP determined from the Coulomb potential (U) of the charged vacancy with $\beta = 1.29$, $U(r) = \beta(\hbar v_F/r)$. **c**, Constant energy dI/dV maps in the vicinity of the vacancy. Top left: map of neutral vacancy taken at -91 meV. The other panels represent maps of the charged vacancy in **a** taken at the energies corresponding to R1 (-91 meV top right), R1' (-25 meV, bottom left) and R2 (50 meV, bottom right). Tunnelling parameters $V_b = -200$ mV, $I = 20$ pA, $V_g = -54$ V.

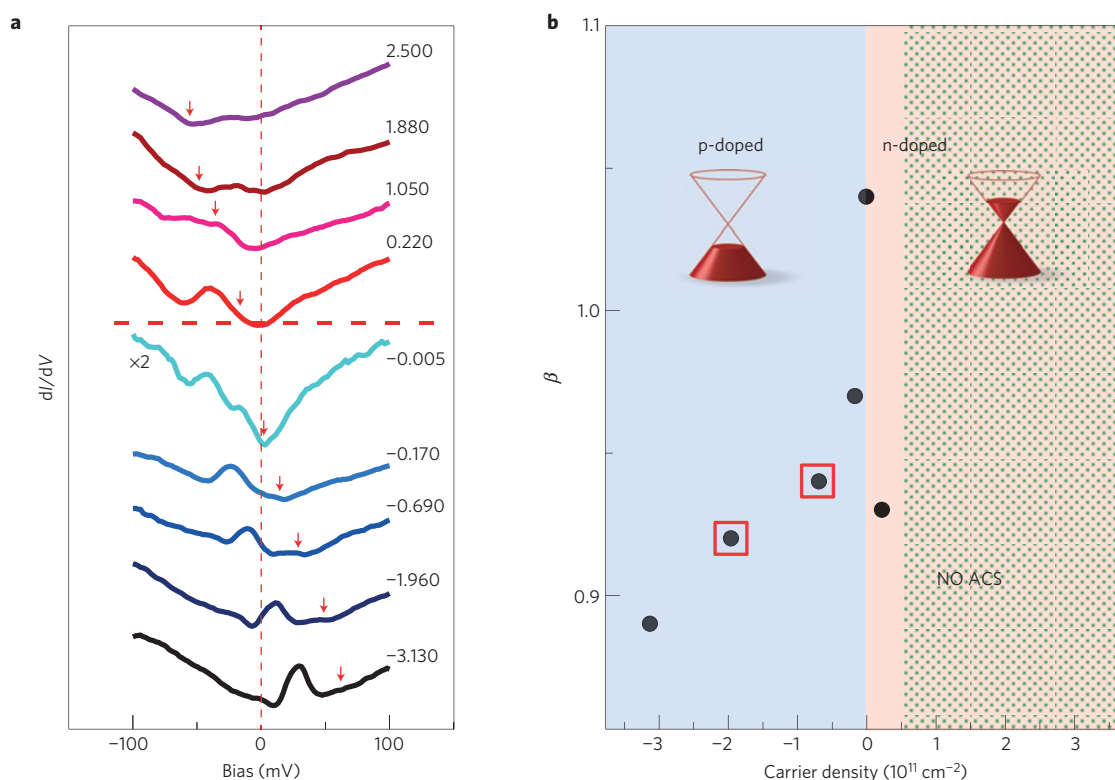


Figure 5 | Gate-dependent screening of AC states. **a**, Carrier density dependence of the AC state. Arrows label the bulk DP measured far from the vacancy. The horizontal dashed line separates the p-doped (below) from the n-doped regime (above) and the vertical dashed line marks E_F . The spectra are labelled by the carrier density expressed in units of 10^{11} cm^{-2} . The carrier density is obtained from the dI/dV curves far from the vacancy: $= (1/\pi)(E_D/\hbar v_F)$, where v_F is extracted from the LL fitting. Tunnelling parameters: $V_b = -100$ mV, $I = 20$ pA. **b**, Evolution of β with carrier density shows the strong electron-hole asymmetry of the screening. The squares mark the regime where the E_F and AC state intersect.

Fig. 5s). On exceeding the critical value, $\beta > 0.5$, a new branch, labelled R1, emerges below the DP. We identify R1 as the counterpart of the 1S AC state in atoms^{12,13}. R1 is clearly distinguishable from the VP by its significantly larger spatial extent (Supplementary Figs 11s and 15s), which reflects its quasi-bound nature^{8,9}. With increasing β , R1 develops a satellite, R1', which tracks its evolution with β . While

R1 is a universal feature of AC states, R1' is due to the locally broken sublattice symmetry and is peculiar to the supercritically charged single-atom vacancy. As β further increases, more branches emerge, starting with R2, which is the equivalent of the 2S AC state⁷⁻⁹.

In Fig. 3 we consider the evolution of the spectra with β . After the first few pulses, the peak, which initially is close to the DP, broadens

and sinks in energy, eventually disappearing below the experimental horizon. This behaviour, together with the fact that the peak remains tightly localized on the vacancy site (Supplementary Fig. 5s), helps identify this peak with the VP branch in the simulation. To obtain the vacancy charge we map the peak energy after each pulse onto the simulated VP in Fig. 3a (symbols in figure). This gives the value of β in the subcritical regime. As the charge is further increased, new peaks emerge below the DP which are qualitatively different from the VP: they are very sensitive to gating and are significantly more spatially spread out, suggesting that they belong to the R1 branch. Mapping their energies onto the R1 branch we obtain β values ranging from $\beta = 0.95$ to 1.29, indicating that the charge is supercritical. Comparing the simulated (Fig. 3b) and measured (Fig. 3c) spectra we find that the AC states gradually emerge with increasing charge, first revealing the R1 state, then its satellite R1' and, finally, for $\beta = 1.29$ all three states R1, R1' and R2 are clearly resolved.

The spatial dependence of the spectra in the AC regime (Fig. 4) shows that, in contrast to the tightly localized VP, the AC states extend far beyond the vacancy site. The DOS enhancement associated with the R1 state (top right of Fig. 4c) consists of a central disk surrounded by an outer halo. Comparing to the local DP (dashed line) in Fig. 4b, we note that, within the central disc, R1 lies above the local DP corresponding to electron states, but it is below the local DP at the halo position, indicating spatially separated electron-hole states. The hole states are absent at energies far from R1, as well as in the subcritical regime which excludes standard energy-resolved Friedel oscillations⁸ (Supplementary Section 10). An alternative interpretation of the electron-hole states is suggested by the analogy with atomic collapse in superheavy nuclei, where vacuum polarization generates electron-positron pairs^{7,8,13,27}.

The doping dependence of the AC state shown in Fig. 5 provides insight into its screening by the itinerant carriers. We find that the screening exhibits strong electron-hole asymmetry. In the p-doped regime the R1 peak persists over the entire experimental range, suggesting poor screening by the positive carriers. In contrast, on the n-doped side the AC peaks disappear rapidly with doping, indicating that screening by negative carriers is very efficient. This unusual screening asymmetry may reflect the charge-induced electron-hole asymmetry in the local DOS (Fig. 5 and Supplementary Fig. 10s), or it could be the result of correlations¹¹, but more work is needed to understand this phenomenon. A direct experimental consequence of the asymmetry is that the AC state can be turned on or off with a modest gate voltage, providing a switching mechanism for localized states. Moreover, the readily implemented charging technique reported here could enable the fabrication of artificial atom arrays for electrostatic control and guidance of electrons in graphene.

Methods

Methods and any associated references are available in the [online version of the paper](#).

Received 1 September 2015; accepted 13 January 2016;
published online 22 February 2016

References

- Katsnelson, M. I., Novoselov, K. S. & Geim, A. K. Chiral tunnelling and the Klein paradox in graphene. *Nature Phys.* **2**, 620–625 (2006).
- Peres, N. M. R., Guinea, F. & Castro Neto, A. H. Electronic properties of disordered two-dimensional carbon. *Phys. Rev. B* **73**, 125411 (2006).
- Ando, T. Screening effect and impurity scattering in monolayer graphene. *J. Phys. Soc. Jpn* **75**, 074716 (2006).
- Das Sarma, S., Adam, S., Hwang, E. H. & Rossi, E. Electronic transport in two-dimensional graphene. *Rev. Mod. Phys.* **83**, 407–470 (2011).
- Kotov, V. N., Uchoa, B., Pereira, V. M., Guinea, F. & Castro Neto, A. H. Electron–electron interactions in graphene: current status and perspectives. *Rev. Mod. Phys.* **84**, 1067–1125 (2012).
- Khalilov, V. R. & Ho, C.-L. Dirac electron in a Coulomb field in (2+1) dimensions. *Mod. Phys. Lett. A* **13**, 615–622 (1998).
- Pereira, V. M., Nilsson, J. & Castro Neto, A. H. Coulomb impurity problem in graphene. *Phys. Rev. Lett.* **99**, 166802 (2007).
- Shytov, A. V., Katsnelson, M. I. & Levitov, L. S. Vacuum polarization and screening of supercritical impurities in graphene. *Phys. Rev. Lett.* **99**, 236801 (2007).
- Shytov, A. V., Katsnelson, M. I. & Levitov, L. S. Atomic collapse and quasi-Rydberg states in graphene. *Phys. Rev. Lett.* **99**, 246802 (2007).
- Fogler, M. M., Novikov, D. S. & Shklovskii, B. I. Screening of a hypercritical charge in graphene. *Phys. Rev. B* **76**, 233402 (2007).
- Wang, Y. *et al.* Observing atomic collapse resonances in artificial nuclei on graphene. *Science* **340**, 734–737 (2013).
- Pomeranchuk, I. & Smorodinsky, Y. On the energy levels of systems with $Z > 1/137$. *J. Phys.* **9**, 97–100 (1945).
- Zeldovich, Y. B. & Popov, V. S. Electronic structure of superheavy atoms. *Sov. Phys. Usp.* **14**, 673–694 (1972).
- Wang, Y. *et al.* Mapping Dirac quasiparticles near a single Coulomb impurity on graphene. *Nature Phys.* **8**, 653–657 (2012).
- Junkermeier, C. E., Solenov, D. & Reinecke, T. L. Adsorption of NH₃ on graphene in the presence of defects and adsorbates. *J. Phys. Chem. C* **117**, 2793–2798 (2013).
- Lehtinen, O. *et al.* Effects of ion bombardment on a two-dimensional target: Atomistic simulations of graphene irradiation. *Phys. Rev. B* **81**, 153401 (2010).
- Chen, J.-H., Li, L., Cullen, W. G., Williams, E. D. & Fuhrer, M. S. Tunable Kondo effect in graphene with defects. *Nature Phys.* **7**, 535–538 (2011).
- Kelly, K. F., Sarkar, D., Hale, G. D., Oldenburg, S. J. & Halas, N. J. Threefold electron scattering on graphite observed with C₆₀-adsorbed STM tips. *Science* **273**, 1371–1373 (1996).
- Ugeda, M. M., Brihuega, I., Guinea, F. & Gómez-Rodríguez, J. M. Missing atom as a source of carbon magnetism. *Phys. Rev. Lett.* **104**, 096804 (2010).
- Andrei, E. Y., Li, G. & Du, X. Electronic properties of graphene: a perspective from scanning tunneling microscopy and magneto-transport. *Rep. Prog. Phys.* **75**, 056501 (2012).
- Yazyev, O. V. & Helm, L. Defect-induced magnetism in graphene. *Phys. Rev. B* **75**, 125408 (2007).
- Pereira, V. M., Guinea, F., Lopes dos Santos, J. M. B., Peres, N. M. R. & Castro Neto, A. H. Disorder induced localized states in graphene. *Phys. Rev. Lett.* **96**, 036801 (2006).
- Liu, Y., Weinert, M. & Li, L. Determining charge state of graphene vacancy by noncontact atomic force microscopy and first-principles calculations. *Nanotechnology* **26**, 035702 (2015).
- Luican-Mayer, A. *et al.* Screening charged impurities and lifting the orbital degeneracy in graphene by populating Landau levels. *Phys. Rev. Lett.* **112**, 036804 (2014).
- Repp, J., Meyer, G., Olsson, F. E. & Persson, M. Controlling the charge state of individual gold adatoms. *Science* **305**, 493–495 (2004).
- Zhao, A. *et al.* Controlling the Kondo effect of an adsorbed magnetic ion through its chemical bonding. *Science* **309**, 1542–1544 (2005).
- Nishida, Y. Vacuum polarization of graphene with a supercritical Coulomb impurity: low-energy universality and discrete scale invariance. *Phys. Rev. B* **90**, 165414 (2014).

Acknowledgements

Funding was provided by DOE-FG02-99ER45742 (STM/STS), NSF DMR 1207108 (fabrication and characterization). Theoretical work supported by ESF-EUROCORES-EuroGRAPHE, FWO-VI and Methusalem programme of the Flemish government. We thank V. F. Libisch, M. Pereira and E. Rossi for useful discussions.

Author contributions

J.M. and Y.J. collected and analysed data and wrote the paper; G.L. built the STM and analysed the data; D.M., M.R.M. and F.M.P. carried out the theoretical work; K.W. and T.T. provided the BN sample. E.Y.A. directed the project, analysed the data and wrote the paper.

Additional information

Supplementary information is available in the [online version of the paper](#). Reprints and permissions information is available online at www.nature.com/reprints. Correspondence and requests for materials should be addressed to E.Y.A.

Competing financial interests

The authors declare no competing financial interests.

Methods

The samples consist of two stacked graphene layers deposited on a hexagonal boron nitride (hBN) flake (G/G/hBN) which rests on a SiO₂ substrate capping an n-doped Si backgate (Fig. 1a). The hBN and bottom graphene layers reduce the substrate-induced random potential fluctuations and help reveal the intrinsic electronic properties of the top layer^{28–30}. The atomic lattices of the two graphene layers are intentionally misaligned to decouple them and to restore the linear spectrum characteristic of single-layer graphene³¹. The decoupling is directly observable with Landau Level (LL) spectroscopy (Supplementary Figs 1s and 2s) through the characteristic \sqrt{NB} dependence of the LL energies expected for single-layer graphene^{20,32}. Here, B is the magnetic field and N the level index. Vacancies were created by sputtering with 100–140 eV He⁺ ions under ultrahigh vacuum conditions followed by high-temperature *in situ* annealing^{16,17}. The effect of the irradiation can be seen in the Raman spectra by the appearance of the D peak, signifying the presence of lattice vacancies (Supplementary Fig. 4s). The STM voltage pulses are typically 2–3 V and ~ 1 –10 s duration. STM spectra are taken with the tip grounded and the bias voltage, V_b , applied to the sample. Multiple vacancies were studied in two samples, which are labelled 1 (Fig. 1) and 2

(Figs 2–5) and their characteristics and gate voltage dependence are described in the Supplementary Information. Furthermore, our studies of pulsed vacancies in graphene supported by other substrates (G/hBN, G/G/SiO₂) produced similar results, as discussed in Supplementary Section 6.

References

28. Dean, C. R. *et al.* Boron nitride substrates for high-quality graphene electronics. *Nature Nanotech.* **5**, 722–726 (2010).
29. Xue, J. *et al.* Scanning tunnelling microscopy and spectroscopy of ultra-flat graphene on hexagonal boron nitride. *Nature Mater.* **10**, 282–285 (2011).
30. Lu, C. P. *et al.* Local and global screening properties of graphene revealed through Landau level spectroscopy. Preprint at <http://arXiv.org/abs/1504.07540> (2015).
31. Li, G. *et al.* Observation of Van Hove singularities in twisted graphene layers. *Nature Phys.* **6**, 109–113 (2010).
32. Li, G., Luican, A. & Andrei, E. Y. Scanning tunneling spectroscopy of graphene on graphite. *Phys. Rev. Lett.* **102**, 176804 (2009).